Analyzing poly(3-hexyl-thiophene):1-(3-methoxy-carbonyl)propyl-1-phenyl-(6,6)C_{61} bulk-heterojunction solar cells by UV-visible spectroscopy and optical simulations

Kristian O. Sylvester-Hvid[a)]
Freiburger Materialforschungzentrum, University of Freiburg, Stefan-Meier-Strasse 21, D-79104 Freiburg im Breisgau, Germany

Tobias Ziegler, Moritz K. Riede, Nicholas Keegan, Michael Niggemann, and Andreas Gombert
Fraunhofer Institute for Solar Energy Systems ISE, Heidenhofstrasse 2, 79110 Freiburg im Breisgau, Germany

(Received 14 March 2007; accepted 12 July 2007; published online 5 September 2007)

A nondestructive method for assessing the thickness of the photoactive layer in poly(3-hexyl-thiophene):1-(3-methoxy-carbonyl)propyl-1-phenyl-(6,6)C_{61} (P3HT:PCBM) solar cells is reported. In the approach the absorption spectrum of the solar cell as derived by optical simulations is fitted to the corresponding measured spectrum, varying only the P3HT:PCBM layer thickness. Within the 50–250 nm thickness range, a linear correlation between the position of a certain spectral minimum and the P3HT:PCBM layer thickness is shown, based on simulated absorption spectra. As an initial application, absorption spectra for 240 P3HT:PCBM solar cells prepared at four different spin-coating speeds were recorded, and the average P3HT:PCBM layer thickness estimated for each spin-coating speed. The simulated fraction of light absorbed in the P3HT:PCBM layer of the solar cells is compared with the P3HT:PCBM absorption spectra measured for films spin coated on simpler substrate types. The latter spectra cannot account for the light harvested in the photoactive layer of P3HT:PCBM solar cells because of substantial optical interference in the solar cells. The measured short circuit current densities J_{sc} for the solar cells vary with the spin-coating speed in a manner confirmed by optical simulations of the maximal short circuit current densities. The measured efficiencies follow the same pattern. On average the measured J_{sc} is 1–2 mA/cm^2 below the simulated maximal short circuit current densities. Based on the resemblance of the measured and simulated absorption spectra such difference can be attributed to recombination exclusively. © *2007 American Institute of Physics*. [DOI: 10.1063/1.2775219]

I. INTRODUCTION

In the understanding of polymer based bulk-heterojunction solar cells and their optimization, the thickness and the light-harvesting properties of the photoactive layer are of particular interests. Both have been the subject of a vast number of studies. A common but somewhat simplified perception is that the thickness of the photoactive layer needs to be large enough to ensure sufficient harvesting of the incident solar radiation, but not too large due to limited mobilities of the materials. As an essential design parameter of organic solar cells, thickness measurements of the photoactive layer for *working* solar cells are, however, rarely reported, as is a correct assessment of the light-harvesting properties of the photoactive layer in the solar cell. The latter property is of particular relevance for estimating the maximal short circuit current, the level of recombination, and the internal quantum efficiency (IQE) of the solar cell. In this study we demonstrate that the thickness of the photoactive layer in poly(3-hexyl-thiophene):1-(3-methoxy-carbonyl)propyl-1-phenyl-(6,6)C_{61} (P3HT:PCBM) bulk-heterojunction solar cells can be derived from the measured reflection spectrum of the solar cell. Further, we show how the light-harvesting properties of the photoactive P3HT:PCBM composite layer (the blend layer) only by means of optical simulations can be correctly analyzed. Finally, we assess the maximal short circuit current density for varying blend thickness, and compare with short circuit current densities measured for P3HT:PCBM solar cells, as prepared with four different blend thicknesses.

Figure 1 illustrates the different types of thin-film structures considered in this study: In Fig. 1(a) the photoactive blend is spin coated directly on substrate glass and a structure obtained which we here refer to as *s* type. In Fig. 1(b) the blend is spin coated on a multilayer structure equivalent to what is used for making the solar cell [shown in Fig. 1(c)], and the resulting structure is here referred to as an *m*-type structure.

Normally when determining the blend thickness for polymer solar cells, the assessment is done indirectly, i.e., by deducing it from fabrication parameters such as the spin-coating procedure employed during solution processing of the blend material. This requires that a correlation between spin-coating conditions and blend layer thickness has been established in advance for a model system, such as the *s*- or

[a)]Electronic mail: See www.sylvesterhvid.dk/kristian. Also at Fraunhofer Institute for Solar Energy Systems ISE, Heidenhofstr. 2, 79110 Freiburg im Breisgau, Germany.

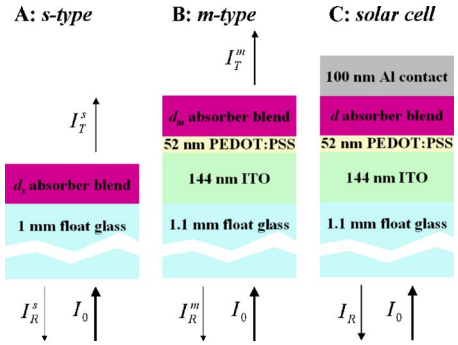

FIG. 1. (Color online) Schematic illustration of the thin-film structures investigated in this study. Of the incident intensity I_0, for the single-layer (*s* type) structure in (a) I_R^s is reflected and I_T^s transmitted. For the multilayer (*m* type) structure in (b) I_R^m is reflected and I_T^m transmitted and for the solar cell structure in (c) an amount of I_R is reflected.

m-type structures. Because the spin-coating process is influenced by many parameters (some of which are difficult to control) such correlations are generally not transferable between laboratories, however. Moreover, in case such correlations are based on an *s*-type structure, *a priori* one cannot assume that a solar cell spin coated under the same conditions will have the same blend layer thickness. For this assumption to hold the *m*-type structure would need to be considered, since only then is the blend spin coated on a surface with similar wetting properties. Irrespective of the structure considered, the blend layer thickness is often measured using microscopic surface probing techniques such as atomic force microscopy (AFM) or profilometry. Because these are local measurements of the blend thickness caution must be exercised, in particular, for *m*-type structures, where substrate layout and/or indium tin oxide (ITO) structuring may cause inhomogeneities in the blend thickness. Further, such measurements are impractical for a large number of solar cells, and in any case do not probe the spatial average of the blend thickness within the electrically active area of the solar cell. We are thus strongly motivated to devise an approach by which the blend thickness can be measured efficiently and nondestructively. This is also of interest for purposes of quality monitoring in future large volume production of polymer solar cells. UV-visible (vis) reflection probe techniques are well known and commercially available, and for simpler thin-film structures routinely used for the simultaneous determination of layer thicknesses and optical constants. For complex and strongly absorbing multilayer systems such as solar cells such standard techniques are not feasible. We have thus implemented a simple and efficient measurement of the reflection spectrum of P3HT:PCBM solar cells. From the corresponding absorption spectrum we have identified a spectral minimum, the position of which correlates linearly with the blend layer thickness. This correlation can be mapped out either by analyzing absorption spectra for P3HT:PCBM solar cells as simulated for a range of blend layer thicknesses or by analyzing the experimental absorption spectra in regard to blend thicknesses as measured by, e.g., AFM. We compare the two approaches and discuss why different correlations are obtained.

The analysis of the light-harvesting properties of the P3HT:PCBM layer upon annealing,[1–9] varying composition,[3,4,10] and spin-coating conditions[3,9,11] is normally based on UV-vis transmission spectroscopy. The spectra are typically recorded for *s*-type structures, and in few cases for *m*-type structures. In either case the data are always reported in terms of an absorption spectrum for the blend.[1] Often it is implicitly assumed that these absorption spectra are representative of the light absorption in the blend while embedded in the solar cell structure. This assumption is not justified as we will show by comparing the UV-vis spectra of *s*- and *m*-type structures with the simulated absorption for the photoactive blend of the solar cell. The reason for this is optical interference in thin-film structures, the effect of which generally increases with the number of thin-film layers and difference between the refractive index of these layers. The structures in Fig. 1 are therefore optically distinct, in particular, the solar cell with its highly reflecting Al back contact. The importance of optical interference for polymer solar cells is already accounted for in numerous studies.[12–24] For P3HT:PCBM solar cells, in particular, where the recombination loss under short circuit conditions can be quite low,[20] the short circuit current density (J_{sc}) is primarily determined by the optical intensity distribution inside the photoactive layer. Optical simulations are therefore suited for investigating the dependence of J_{sc} on blend layer thickness, either assuming an IQE of unity[16,18,19] giving J_{sc}^{max} or by coupling to electrical simulations,[19,20] and thus approximating J_{sc}. In either case an undulating behavior for J_{sc} versus blend layer thickness is generally obtained[16,18] as also experimentally confirmed by several studies.[15,16,19,20] However, in these studies the film thicknesses were all deduced from AFM or profilometry measurements on either *s*- or *m*-type structures. Here we complement the literature by analyzing the dependence of J_{sc}^{max} on blend layer thickness by means of optical simulation, and by comparing this with J_{sc} measured for 240 P3HT:PCBM solar cells prepared at four different spin-coating speeds. This comparison allows a rigorous assessment of the level of recombination for the P3HT:PCBM solar cells prepared.

II. EXPERIMENT

A. Sample preparation

For 240 solar cells prepared on 24 substrates only the spin-coating speed was varied while taking extra measures to keep all other process parameters unchanged. No effort was taken to optimize the efficiency: We simply used the process parameters reported in the literature claimed to result in 4%–5% efficiency.[4,6,11,25] 1.1 mm ITO glass (Merck 20 Ω/□) was laser ablated to yield an ITO structure with ten anode pixels within a substrate area of 25×25 mm^2. The pixel layout allows for four-probe *IV* characterization once the metal cathode is deposited. The substrates were first manually washed in aqueous detergent, and then sequentially sonicated for 10 min twice in acetone, isopropanole, and deionized water. Handling of the substrates during and after cleaning was done in a clean room facility where they were

[1]I.e., corrected for the absorption of the bare substrate be that *s*- or *m*-type.

subsequently blow dried with N_2 and UV ozone treated for 20 min. With as little delay as possible following this treatment, the substrates were spin coated with a poly(3,4-ethylenedioxythiophene):poly(styrene sulfonate) (PEDOT:PSS) suspension (Baytron AI4083) for 60 s at 3000 rpm, filtering the PEDOT:PSS dispersion through a 0.45 μm filter. The substrates were dried for 10 min at 200 °C and subsequently transferred under a glass cover directly to a dry N_2 glove box environment (H_2O less than 2 ppm and O_2 less than 1 ppm) where all subsequent steps were conducted. The blend layer was applied by spin coating 70 μL P3HT:PCBM solution per substrate using a procedure with either 630, 900, 1430, or 1970 rpm,[26] and spinning times past drying of the blend as indicated by the sudden color change. The P3HT:PCBM solution as prepared in advance consisted of 15 mg/ml P3HT (4002E, Rieke Metals, used as received) and 10.5 mg/ml PCBM (Solenne BV, used as received) dissolved in anhydrous *o*-dichlorobenzene and stirred for more than 24 h at 40 °C and subsequently filtered through 0.45 μm PTFE filters. Following blend spin coating, the substrates were stored under low vacuum for ~24 h and subsequently transferred to the evaporation chamber. Approximately 100 nm Al was deposited at a base pressure of less than 5×10^{-6} mbar over 10 min, with a rate of ~0.1 nm s^{-1} for the first 5 nm. The evaporation mask defined a cathode area of 5.3 mm^2 for each of the ten solar cells on a substrate, and the eight substrates loaded simultaneously into the vacuum chamber defined a batch. All through substrate processing, apart from the spin-coating steps, these batches were processed simultaneously to reduce unintentional scatter in the process parameters. The *m*-type substrates were fabricated in the same manner but using unstructured ITO glass and omitting the final Al deposition step. Note that transmission spectra were recorded between PEDOT:PSS and blend spin coating for the *m*-type substrates. For the *s*-type substrates P3HT:PCBM solution was spin coated directly onto 1 mm float glass after cleaning and UV-ozone treatment. For both *s*- and *m*-type substrates, two identical substrates were prepared at each spin-coating speed resulting in eight samples of each type. Irrespective of the substrate type, temperature annealing was performed by heating substrates at 150 °C for 5 min on a temperature controlled hot plate inside the glove box.

B. Transmission and reflection measurements

The reflection spectra of *m*-type structures and solar cells were all recorded at normal incidence. An Avantes charge-coupled device (CCD) spectrometer with 2048 pixels (AvaSpec-2048, 325–1100 nm range) and an Avantes halogen/deuterium light source (AvaLight-DHc, 400–1700 nm/200–400 nm ranges) were used and connected via a bifurcated optical fiber to a reflection probe, equipped with a collimating lens placed ~5 cm away from the sample. The reflection spectra were generally recorded for 200 ms and averaged over ten spectra. Reference spectra were recorded in the same geometry using a freshly vacuum deposited Al mirror (>100 nm and facing the light). The incident light was focused to a spot with a diameter of ~1 mm and centered with respect to the round solar cell pixel. Great care was taken to correct for even small deviations away from normal incidence. The reflection was calculated as

$$R=\frac{I_R-I_d}{I_0-I_d}=\frac{I_R-I_d}{R_{\mathrm{Al}}^{-1}I_0'-I_d}, \tag{1}$$

where I_0 and I_R are the incident and reflected intensities [Fig. 1(c)], I_0' the intensity reflected by the Al mirror, I_d the dark signal of the spectrometer, and R_{Al} the reflectivity for an Al surface.[27] For the solar cells (only) the absorption was derived as $A=1-R$. All reflection measurements were performed in the glove box. The *s*- and *m*-type samples had their transmission spectra recorded with an AnalyticJena Specord 210 spectrometer (190–1100 nm range) at normal incidence and under ambient conditions.

C. Other measurements

The solar cells had their current-voltage characteristics measured under a linear voltage sweep between ±1 V in the dark and under approximate AM 1.5 illumination with 1000 W m^{-2} (Steuernagel Solar Test) corrected for spectral mismatch (for the calibrated Si-reference diode the mismatch factor was 1.09). The measurements were made in the glove box under constant temperature.

The optical constants (n,k) for the annealed blend were determined from the *s*-type substrates by measuring the ellipsometric constants at incidence angles of 40°, 50°, 60°, 70°, and 80° using an ellipsometer from J. A. Woollam (M-2000U). At each angle 250 measurements were performed between 250 and 1000 nm. Prior to measurement the backside of the samples were roughened to avoid reflections from the back surface. The resulting ellipsometric constants were fitted to an optical model consisting of a Cauchy layer of variable thickness (representing the blend layer) on a 1 mm float glass substrate. This was done for each substrate for wavelengths between 750 and 1000 nm using the software WVASE32, which yielded blend layer thicknesses for the different spin-coating speeds as listed in Table I. Subsequently, using these thicknesses and the Cauchy parameters determined for each *s*-type substrate, the *average* optical constants for the blend were obtained through a fitting procedure involving data from all eight substrates, again using WVASE32. In a similar manner, optical constants for PEDOT:PSS were determined using PEDOT:PSS from the same product batch as used for preparing the *m*-type substrates. The measurements were done under ambient conditions.

AFM measurements were performed using a calibrated Veeco Nanoscope IV in tapping mode scanning a rectangular box of 3×50 μm^2 under ambient conditions. This scan box was typically placed over one of the edges of an ~0.2 mm scratch made on the blend film, and the vertical step profile evaluated at three positions. Such measurements were repeated at least for two different positions on the substrates. For *s*-type substrates simple step profiles were consistently obtained, the heights of which are listed in Table I. By carefully searching the edges of the scratches on the *m*-type substrates, double-step profiles due to only partial removal of

TABLE I. Blend layer thicknesses (in nm) as determined for the different substrates prepared at four spin-coating speeds. For *s*-type substrates average values are given for thicknesses determined by AFM and ellipsometry. For *m*-type substrates average values with the standard deviations are given for thicknesses determined by AFM. For thicknesses derived by spectral fitting, labels *t* and *r* denote, respectively, if the transmission or reflection spectrum was used. Also shown are the PEDOT:PSS layer thicknesses obtain from spectral fitting and AFM.

Substrate type	Spectral fitting	AFM	Ellipsometry
s type	*t*		
630 rpm	121	145/141	152.49/149.21
900 rpm	99	121/131	127.29/127.46
1430 rpm	80	103/98	···/99.74
1970 rpm	69	83/86	80.79/83.09
m type	*t*/*r*		
630 rpm	119/137[a]	154±7	···
900 rpm	103/110[a]	125±1	···
1430 rpm	84/84	84±5	···
1970 rpm	57/56	76±2	···
Solar cell	*r*		
630 rpm	122	···	···
900 rpm	100	···	···
1430 rpm	76	···	···
1970 rpm	62	···	···
PEDOT:PSS	*t*		
3000 rpm	52	47±4	

[a]Spectral fitting was of low quality.

the harder PEDOT:PSS layer could be identified for all substrates. This conveniently allowed for measuring the PEDOT:PSS and blend layer thicknesses during the same scan, the values of which are also shown in Table I. In all cases the AFM scans were conducted at the center of the substrates where the transmission spectra were recorded.

III. OPTICAL SIMULATIONS

Optical simulations were performed using two approaches. In the first the *S* matrix formalism as appropriate for the one-dimensional analysis of planar stacked thin-film structures is implemented as a graphical tool. With this the transmission or reflection spectrum for the entire substrate can be simulated for varying layer thicknesses, and compared with a corresponding experimental spectrum. Hence, by visual inspection we can match a simulated spectrum to an experimental spectrum adjusting one or more layer thicknesses. This fitting is done manually by seeking the best superimposition of the spectra, in particular, for features such as extrema within the 300–750 nm range. The obtained layer thicknesses are therefore not found in a mathematically strict sense. However, within an uncertainty of a few nanometers, the best fit was generally quite obvious. In the following, we refer to this procedure as *spectral fitting*.

In the second approach we used the more general rigorous coupled wave analysis tool as developed for optical simulations of corrugated films.[28–32] Here we used its capabilities to compute the spatially resolved absorption density. From this the total absorption spectrum of a solar cell, the absorption in the blend layer, and the maximal current density J_{sc}^{max} (assuming IQE=1) can be derived. Below we refer to such simulations as *optical simulations*.

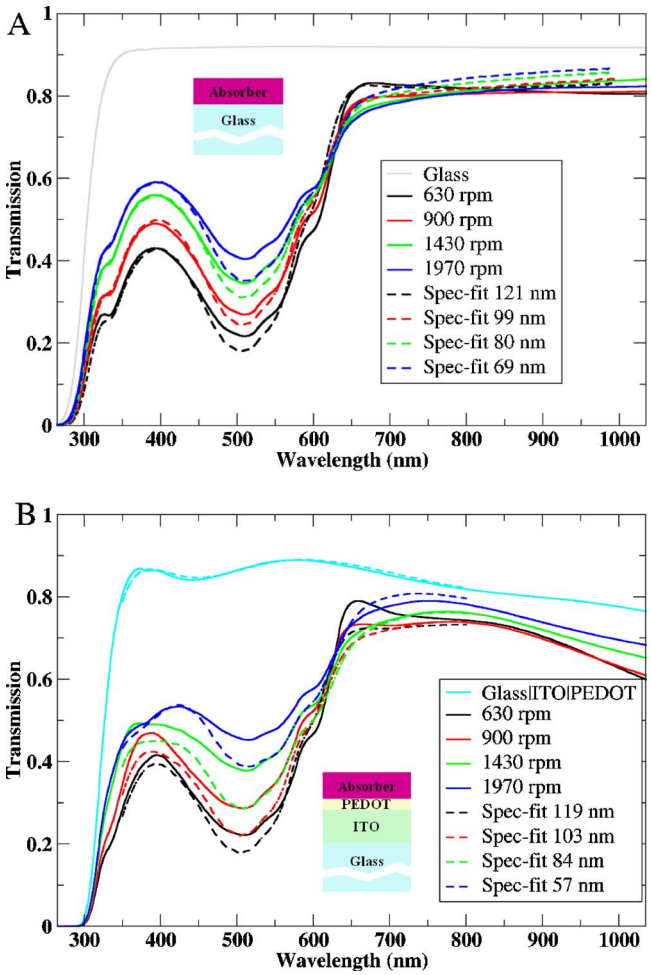

FIG. 2. (Color online) Transmission spectra obtained for (A) single-layer substrates (*s* type) and (B) multilayer substrates (*m* type) prepared at different spin-coating speeds. For comparison spectra for the glass substrate (A) and PEDOT:PSS coated ITO glass (B) are shown. Dashed lines represent spectra derived from spectral fitting of the measured transmission spectra. Spectral fitting of the average glass|ITO|PEDOT:PSS spectrum (B) yielded layer thicknesses of 144 nm for ITO and 52 nm for PEDOT:PSS.

To determine the thickness of the ITO and PEDOT:PSS layers first spectral fitting of the glass|ITO transmission spectrum was done resulting in an ITO thickness of ~144 nm. Using this value, spectral fitting of the glass|ITO|PEDOT:PSS average transmission spectrum gave ~52 nm for the PEDOT:PSS layer thickness.[2] The glass|ITO|PEDOT:PSS transmission spectrum in Fig. 2(b) is an average spectrum based on eight identically prepared substrates (which after blend spin coating became *m*-type substrates).

Next, spectral fitting was performed for all types of spectra, measured for every structure in Fig. 1 in order to determine the blend layer thicknesses resulting from different spin-coating speeds. The results are shown in Table I where *t* and *r* label whether a thickness results from spectral fitting of the transmission or reflection spectrum. The corresponding

[2]Note that spectral fitting of the individual glass|ITO|PEDOT:PSS transmission spectra showed a variation in the PEDOT:PSS layer thickness of less than a few nm.

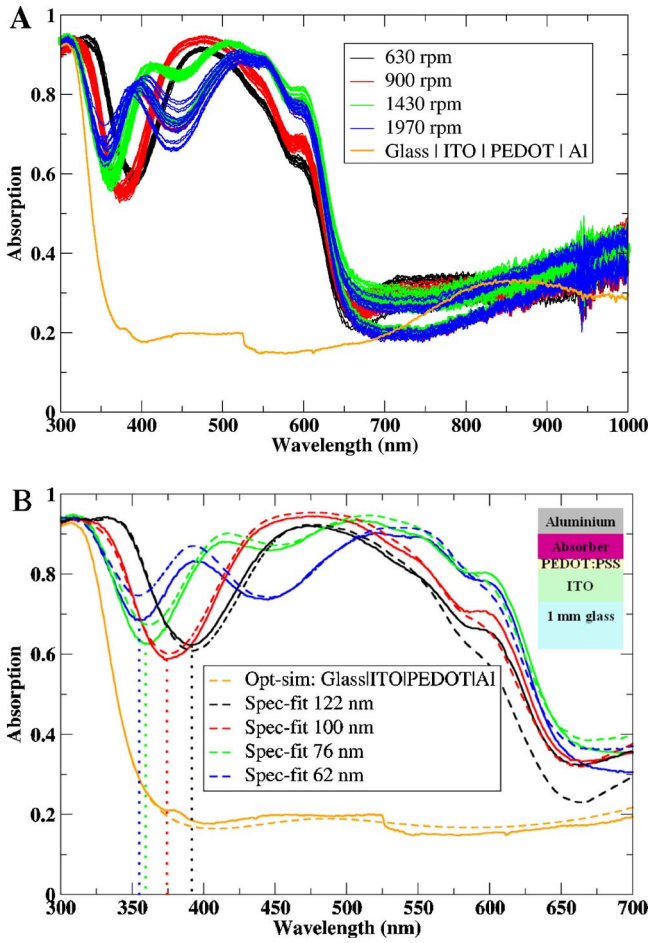

FIG. 3. (Color online) Shown in (A) are the absorption spectra measured for the individual solar cells prepared at four different spin-coating speeds. Also shown is the average spectrum obtained for glass|ITO|PEDOT:PSS|Al structures. Shown in (B) are the absorption spectra obtained from averaging over all solar cells prepared at the same spin-coating speed, along with the average glass|ITO|PEDOT:PSS|Al spectrum. Dashed lines represent the corresponding simulated spectra obtained from spectral fitting. Vertical lines mark the position of λ_{min} as identified for different spin-coating speeds.

fitting spectra are shown with dashed lines in Fig. 2 for *s*- and *m*-type substrates and in Fig. 3(b) for the solar cells. The reflection spectra for the *m*-type structures are not shown, however.

Optical simulations were performed for the solar cell structure [Fig. 1(c)] at normal light incidence in the 300–800 nm wavelength range in steps of 2 nm, varying the blend layer thickness as 50, 60, and 70, ... ,250 nm, and using 144 nm ITO, 52 nm PEDOT:PSS, and 100 nm Al. Similar simulations were done using the four blend layer thicknesses determined from spectral fitting of the average experimental absorption spectra of the solar cells (Table I). Optical constants for P3HT:PCBM and PEDOT:PSS were those as determined by ellipsometry, whereas for ITO and aluminum tabulated values were used.[27]

IV. RESULTS

Below we present the results for *s*- and *m*-type substrates and solar cells with different thicknesses of the blend layer. For convenience we reference the different thicknesses loosely by the spin-coating speeds employed, and stress that all determined thicknesses are listed in Table I.

In Fig. 2 the transmission spectra (solid lines) recorded for the *s*- and *m*-type substrates with the blend deposited at the four spin-coating speeds are shown. Generally two absorption peaks are observed, namely, a dip from P3HT between 400 and 650 nm and a dip starting at 350 nm due to PCBM, both in correspondence with the thin-film spectra of the pure materials.[2] The most notable difference between Figs. 2(a) and 2(b) is the way in which the transmission spectra for increasing spin-coating speeds (decreasing blend layer thickness) are displaced with respect to each other. For the *s*-type substrates [Fig. 2(a)], the transmission between 300 and 650 nm generally increases with spin-coating speed but with the spectral shape being unchanged, whereas for the *m*-type substrates the spectral shape changes with increasing spin-coating speed. Hence, in this wavelength range the *s*-type structures show no interference and the *m*-type structures show beginning signs of interference, which become more pronounced with decreasing layer thickness. Between 650 and 800 nm, both *s*- and *m*-type substrates are influenced by interference as evidenced by an *increasing* transmission with increasing blend layer thickness.

Spectral fitting reproduces the *s*-type transmission spectra reasonably well for all spin-coating speeds as seen in Fig. 2(a), although the P3HT absorption is slightly underestimated. The resulting blend thicknesses are listed in Table I along with the corresponding values obtained from the Cauchy model and from AFM measurements. Spectral fitting qualitatively reproduces the *m*-type transmission as seen from Fig. 2(b). Features such as the displacement of the maximum at ~400 nm with increasing spin-coating speed is accounted for, but also here the P3HT peak is underestimated. Spectral fitting of the *m*-type reflection spectra (not shown) worked well for the 1430 and 1970 rpm cases but failed to reproduce significant spectral features in the remaining cases. Blend thicknesses resulting from the fitting of transmission and reflection spectra are listed in Table I along with the corresponding AFM values.

Figure 3(a) shows the absorption spectra for the solar cells as derived from the corresponding measured reflection spectra. By specifically plotting each spectrum, a simple graphical representation of the spread in the absorption data is obtained. Despite a vertical spread among spectra for identically prepared cells, spectral features such as the positions of the extrema between 300 and 500 nm are hardly affected. Comparing the spectra we see that each spin-coating speed has a distinct spectral fingerprint, and that the spread among spectra obtained for a given speed is diminished with decreasing spin-coating speed.

For comparison the average absorption spectrum obtained from 80 glass|ITO|PEDOT:PSS|Al structures is also shown in Fig. 3(a). These samples were prepared identically to the solar cells but without blend. We observe the glass cutoff starting at ~350 nm, a small absorption peak at ~370 nm, and a broad infrared peak due to ITO. The PEDOT:PSS absorption between 400 and 500 nm is hardly visible due to a kink at 526 nm which is an artifact of the measurement setup. To test the quality of *n* and *k* for the

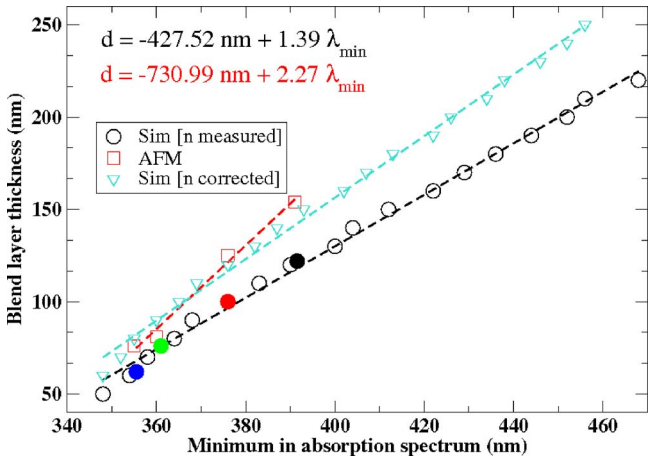

FIG. 4. (Color online) Blend layer thickness vs λ_{min} for measured and simulated solar cell absorption spectra. Solid circles denote (d,λ_{min}) obtained from spectral fitting of measured absorption spectra for solar cells spin coated at 630 (black), 900 (red), 1430 (green), and 1970 rpm (blue). Open circles denote (d,λ_{min}) obtained from optical simulation of absorption spectra with d in the 50–250 nm range. Open boxes designate (d,λ_{min}) where d is determined by AFM on m-type substrates (i.e., d_m) and λ_{min} comes from the measured absorption spectra. Open triangles denote (d,λ_{min}) obtained from optical simulation of the absorption spectra using $(0.85n,k)$. Linear fits are shown with dashed lines.

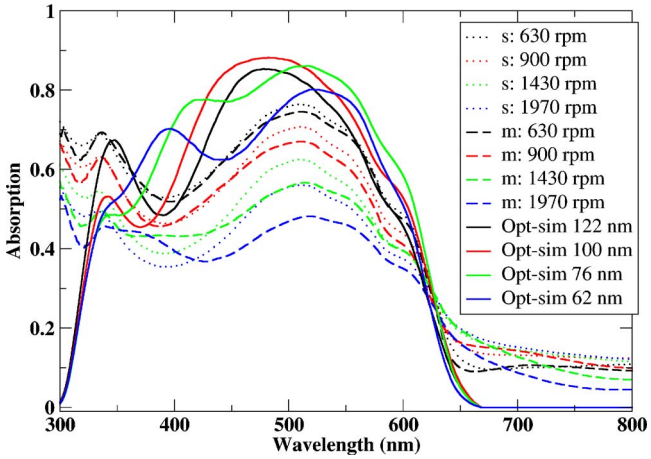

FIG. 5. (Color online) Blend absorption spectra obtained from the corresponding transmission spectra of s-type (dotted lines) and m-type (dashed lines) substrates prepared at different spin-coating speeds. Shown also are the simulated absorption spectra (full lines) for the blend layer in solar cells with thicknesses corresponding to the four spin-coating speeds. The blend thicknesses are found from spectral fitting.

materials *other* than blend, the glass|ITO|PEDOT:PSS|Al absorption spectrum was simulated. On a different scale, in Fig. 3(b) the measured and simulated spectra are compared. Qualitative agreement is observed [also in the region not shown in Fig. 3(b)] although the peak at ~370 nm is missing.

Also shown in Fig. 3(b) are the average absorption spectra for solar cells prepared at the same spin-coating speed. These are compared with the corresponding simulated spectra obtained from spectral fitting. The shown characteristic minima in Fig. 3(b) all move toward longer wavelength with increasing blend layer thickness, hence λ_{min}=391 nm (630 rpm), 376 nm (900 rpm), 361 nm (1430 rpm), and 355 nm (1970 rpm). This trend is confirmed by the optical simulation of solar cell absorption spectra with the blend thickness d varying in the 50–250 nm range. In Fig. 4, we show the corresponding values for λ_{min} vs d (open circles), where linear regression on these data yields a linear fit (dashed line) with a correlation coefficient of 0.9977.

To illustrate that the light-harvesting properties of the blend layer in the solar cells cannot be analyzed in terms of the s- and m-type substrates, in Fig. 5 the blend absorption spectra obtained for these substrates are compared with the blend absorption as *simulated* for solar cells. For the s- and m-type substrates the absorption spectra are derived from the transmission data shown in Fig. 2 by correcting for the substrate absorption and neglecting the reflection contribution, $I_R^{s,m}$.[3] The latter is evident from what seems to be a base line absorption of ~10% above 700 nm in Fig. 5, which is due to reflection as k for the blend vanishes in this region. The simulated absorption spectra (solid lines in Fig. 5) give the fraction of light absorbed in the blend layer of the solar cell with d equal to the values obtained from the spectral fitting [Fig. 3(b)]. Note that these spectra are not normal absorption spectra: they give the absorption of the blend layer subject to the optical constraints of the entire solar cell structure. Noticeable differences compared to the s- and m-type absorption spectra are seen from Fig. 5; the P3HT peak is larger, an additional peak at ~400 nm appears, and finally absorption at the low-wavelength side of the PCBM peak (~350 nm) does not occur.

To assess the upper limit of J_{sc} for the solar cells, blend absorption densities for d in the range 30–250 nm were simulated and J_{sc}^{max} subsequently derived. $J_{sc}^{max}(d)$ is plotted in Fig. 6 and vertical lines marked the blend thicknesses corresponding to the four different spin-coating speeds employed.

To illustrate the electrical performance under illumination of the (working) solar cells fabricated at the four differ-

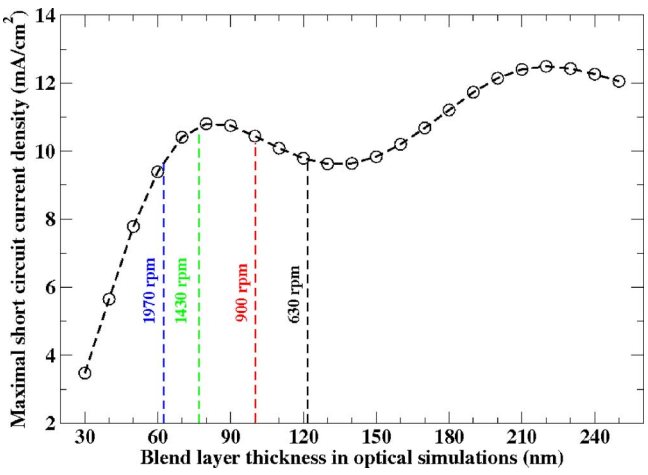

FIG. 6. (Color online) Maximal short circuit current density J_{sc}^{max} vs blend layer thickness as obtained from optical simulations performed for solar cell structures with blend layer thicknesses ranging between 30 and 250 nm. Vertical lines indicate the thicknesses for which the simulated solar cell absorption spectra fit the corresponding measured absorption spectra

[3]The blend transmission is $T_b=T_{b+s}/T_s$, where T_{b+s} is the measured transmission for s- or m-type structure and T_s the corresponding transmission for the bare substrate. Neglecting reflection we have $A=1-T$.

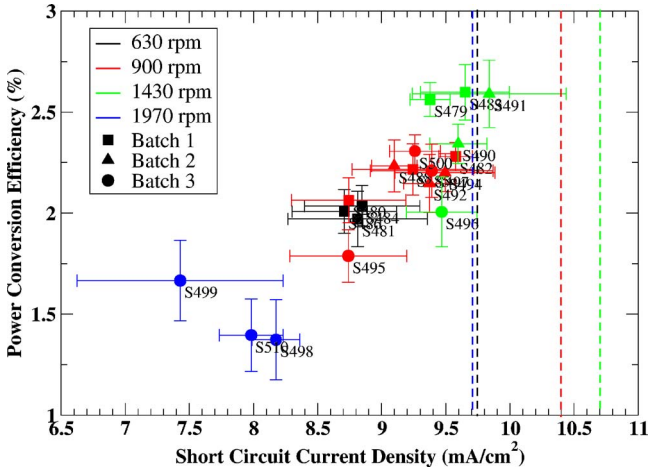

FIG. 7. (Color online) Scatter plot showing the average values (with symbols) and the standard deviations (with error bars) of η vs J_{sc} for the functional solar cells. Different symbols denote the three different fabrication batches. Shown with vertical lines (same color coding) are J_{sc}^{max} derived from optical simulations.

ent spin-coating speeds, in Fig. 7 the efficiency η vs J_{sc} is shown. Symbols mark average values for (η, J_{sc}) obtained for solar cells on the same substrate (substrate number shown) and error bars show the per-substrate standard deviation. Despite a relatively large scatter in both η and J_{sc} for identically prepared substrates, there still seems to be a grouping of substrates prepared at the same spin-coating speed. Both η and J_{sc} increase on changing the spin-coating speed as $1970 \rightarrow 630 \rightarrow 900 \rightarrow 1430$ rpm. Also shown with vertical lines in Fig. 7 are values of J_{sc}^{max} corresponding to the four spin-coating speeds. Not all prepared solar cells are presented in Fig. 7 because some cells simply failed as photovoltaic devices.[4]

V. DISCUSSION

Absorption spectra for functional and electrically characterized P3HT:PCBM solar cells have previously only been reported by Schilinsky *et al.*[33] and Hoppe *et al.*[21] In the latter case the optical constants were fitted to experimental spectra resulting from different postproduction treatments. Fitting the blend layer thickness has not been done so far. This is remarkable considering the sensitivity of λ_{min} with respect to changes in the blend layer thickness, the number studies devoted to optimizing the thickness,[15,16,18,20,25] and the simplicity of the technique. Our results show that even a change of less than 15 nm ($1970 \rightarrow 1430$ rpm) in blend thickness (based on fitted thicknesses) leads to significant changes in the absorption spectrum [Fig. 3(b)]. The spread in the position of λ_{min} in spectra resulting from solar cells made at the same spin-coating speed [Fig. 3(a)], typically lies within a few nanometers; i.e., a shift of $\sim$15 nm in λ_{min} is significant.

The linearity between λ_{min} and the blend layer thickness can be rationalized by the condition of destructive interference between the partial waves transmitted (reflected) at each of the interfaces. Phase differences between the partial waves are introduced both by transmission (reflection) at interfaces and by differences in optical path length. The latter implies that the wavelength at which an interference minimum occurs is proportional to any of the layer thicknesses in the multilayer thin-film system. In the present case, only the blend layer thickness d is varied and the linear relation

$$d(\lambda_{min}) = b + a\lambda_{min} \tag{2}$$

can be mapped. We have observed such linearity also in simulations of other types of solar cells, provided a spectral minimum can be clearly identified in the absorption spectrum.

Figure 4 shows that the coefficients obtained for the linear correlation in Eq. (2) depend on how we assess the blend layer thickness. Which approach is more correct is not immediately obvious because all thickness assessments are indirect. For the AFM case (red boxes in Fig. 4) thicknesses are measured for the m-type substrates (d_m approximates d) and not for the working solar cells. Note that AFM blend thickness measurements for the solar cells (i.e., through the Al cathode) were attempted but lead to inconclusive results. The standard deviations for the AFM determined thicknesses in Table I cannot explain the discrepancy between the two linear relations in Fig. 4. A similar discrepancy between thicknesses determined from AFM and spectral fitting is seen for the s-type substrates (Table I), where the latter numbers are consistently smaller than the corresponding AFM and ellipsometry numbers. Note further the close agreement between AFM and ellipsometry thicknesses determined for s-type substrates.

To assess if the consistently smaller thicknesses as determined by spectral fitting are attributable to problems in the optical constants for the blend, the simulations leading to the open circles in Fig. 4 were repeated for $n \pm 15\%$ and for $k \pm 15\%$. Varying k generally changed only the size and not the positions of the extrema for the simulated spectra. Conversely, varying n changed the position of λ_{min} and thus the coefficients in Eq. (2). Hence, in Fig. 4 we have additionally shown the linear relation obtained from optical simulations using $0.85n$ and k unchanged. The quality of the spectral fitting of the average solar cell absorption spectra was hardly influenced by scaling n, but the agreement with the AFM based linear correlation improved. However, the modified correlation is still not within the standard deviation of the AFM thicknesses. A further decrease of n does not improve the agreement, and in any case cannot be justified in terms of the uncertainty for the optical constants. Redoing the spectral fitting of the s- and m-type transmission spectra using $0.85n$ does not significantly change the thickness assessment for the s- and m-type substrates, in accordance with interference being less important for these substrates.

The above findings indicate a small but seemingly systematic error in the optical constants of the blend. The origin of this can have several sources, the most notable being that the ellipsometric constants were fitted according to an isotropic model. For poly(3-octylthiophene) films anisotropy for the optical constants has been reported.[34] Also, the optical

[4]For those failing for no obvious reasons (bubbles in or partial coverage of the pixel area) the absorption spectra appeared identical to those of the functional solar cells. Figure 3(a) includes therefore also nonfunctional solar cells.

constants were determined by fitting ellipsometric data determined from samples with different blend thicknesses. It is known that different blend layer thicknesses may result in different film morphologies, and thus the average optical constants determined here might not be equally suited for the entire range of thicknesses investigated, as also concluded by Monestier *et al.*[20] This might also explain why spectral fitting of the *m*-type reflection spectra gave poor results for the 630 and 900 rpm cases only (Table I). Finally, assuming the blend to be anisotropic (or uniaxially anisotropic), measuring the ellipsometric constants between 40° and 80° relative to normal incidence might not yield optical constants with sufficient precision to represent the normal incidence situation considered here.

We do not believe that the optical constants for PEDOT:PSS and/or ITO are responsible for the discrepancy in the thickness determinations since the glass|ITO|PEDOT:PSS transmission spectrum [Fig. 2(b)] was reproduced well with 52 nm PEDOT:PSS (47±4 nm from AFM) and the glass|ITO|PEDOT:PSS|Al absorption spectrum likewise [Fig. 3(b)]. Moreover, the discrepancy in the thickness determination also occurs for *s*-type substrates involving blend and glass only. To obtain a better calibration of Eq. (2), the optical constants of the blend need to be measured considering the above issues, which is currently being undertaken. However, regardless of the thickness determination used, the results in Fig. 4 still serve as illustration and proof of concept.

Since the solar cell absorption spectrum does not show where in the thin-film system light is absorbed, using the glass|ITO|PEDOT:PSS|Al or the glass|ITO|PEDOT:PSS spectrum[33] as reference in deriving the fraction of light absorbed in the blend region is not correct. Instead the absorption density for the blend layer should be simulated as done here and by others.[18,21] On comparing the simulated blend absorption with the absorption spectra based on the *s*- or *m*-type substrates [Fig. 5] it is clear that neither of these structures should be used to study the optics of the blend layer in the solar cell. Most clearly this is seen from the peak around 400 nm for the simulated blend absorption (thinnest blend layer: 62 nm), which lacks in the *s*-type absorption spectra and only emerges in the spectrum for the thinnest *m*-type substrate. These spectral differences illustrate the effect of the different electromagnetic field distributions in solar cell and *m*- and *s*-type structures. Nonetheless, in many studies J_{sc}^{max} is estimated from absorption spectra of *s*- or *m*-type structures. This is problematic while as seen from Fig. 5, the *s*- or *m*-type spectra underestimate the absorption inside the spectral range, where current is generated, and overestimate the absorption outside, the latter, in particular, if $I_R^{s,m}$ is not corrected for.

From Fig. 7 it is clear that J_{sc} measured for the solar cells on average is between 1 and 2 mA/cm^2 below the corresponding maximum values J_{sc}^{max}, as simulated for the respective spin-coating speeds. The difference $(J_{sc}^{max}-J_{sc})$ generally has both an optical and an electrical origin, the latter often being the only term considered. By ensuring that the measured and simulated absorption spectra for the solar cells actually match [Fig. 3(b)], within the precision of the optical constants, we here may attribute the difference to recombination only. From $J_{sc}^{max}(d)$ in Fig. 6 we expect J_{sc} to increase with spin-coating speed as 1970→630→900→1430 rpm, with J_{sc} at 630 and 1970 rpm being nearly equal. Experimentally this sequence is also found, but from Fig. 7 we see that solar cells spin coated at 1970 rpm on average give J_{sc} notably smaller than those spin coated at 630 rpm. The difference in J_{sc} must imply more recombination for the thinnest cells, which, however, contradicts the normal behavior of recombination increasing with blend thickness. The steepness of $J_{sc}^{max}(d)$ at small thicknesses (Fig. 6) implies that miscalculating the blend thickness by 5 nm may change J_{sc}^{max} up to ~1 mA/cm^2; i.e., the 1970 rpm solar cells should, in fact, be thinner than 62 nm. This is contradicted by the AFM determined thickness of 76 nm (Table I) for the 1970 rpm case. Hence, the observed difference in J_{sc} for the 630 and 1970 rpm solar cells is not fully understood. Here we can only infer that the 1970 rpm cells overall are more prone to errors and have larger spread in both (η, J_{sc}) and absorption data.

$J_{sc}^{max}(d)$ as shown in Fig. 6 is nearly identical to what Hoppe *et al.*[16] obtained for P3HT:PCBM with ratio 1:0.8 instead of 1:0.7 as used here. As opposed to us, they measured J_{sc} close to J_{sc}^{max} for solar cells with thicknesses around the first maximum at ~85 nm of $J_{sc}^{max}(d)$. Here the best performing solar cells are obtained if spin coating at 1430 rpm (Fig. 7), which corresponds to a blend thickness of 76 nm based on spectral fitting or 84 nm based on AFM. For either value we are still near the first maximum of $J_{sc}^{max}(d)$ (~10.8 mA/cm^2 from Fig. 6) which on average is ~1 mA/cm^2 larger than J_{sc} measured. Experimentally $J_{sc}(d)$ has only been mapped for the 1:1 P3HT:PCBM blend ratio. Li *et al.*[25] found an optimum thickness of 63 nm for both η (4%) and J_{sc} (10.6 mA/cm^2), Moule *et al.*[15] the first maximum of J_{sc} at 110 nm with η~4% and J_{sc}~8 mA/cm^2, and Monestier *et al.*[20] the maximum at ~75 nm with J_{sc} ~10 mA/cm^2. Even among studies employing the same P3HT:PCBM ratio, the experimental determination of the first maximum of $J_{sc}(d)$ is subject to a large spread. Regarding the second maximum of $J_{sc}(d)$, in a different publication Li *et al.* reported η=4.4% and J_{sc}=10.6 mA/cm^2 for solar cells with optimized thicknesses of 210–230 nm,[11] whereas Moule *et al.*[15] found the optimum at 225 nm with η=3.7% and J_{sc} around 10 mA/cm^2. In both cases J_{sc} is substantially smaller than 12.6 mA/cm^2 obtained for J_{sc}^{max} at ~220 nm [Fig. 6], being a clear signature of recombination for large blend layer thicknesses.

We are not able to reproduce the recently acclaimed 4%–5% efficiency,[6,35,36] one reason being due to recombination which affects J_{sc} and thus also η. More detrimental for η are, however, the rather low open circuit voltages (maximum of 550 mV for cells spin coated at 1430 rpm) and fill factors (maximum of 0.51 for cells spin coated at 1430 rpm) obtained for the solar cells in this study.

The blend layer thicknesses derived from spectral fitting (Table I) show that for a given spin-coating speed, qualitatively the same thickness is obtained irrespective of substrate type used. However, this is contradicted by the variation among the thicknesses determined by AFM for the *s*- and *m*-type substrates. Based on the data in Table I we cannot

conclude if the use of *s*-type substrates for establishing relations between spin-coating speed and blend layer thickness is appropriate for P3HT:PCBM solar cells or not.

VI. CONCLUSION

We have measured the reflection spectra of P3HT:PCBM solar cells, derived the corresponding absorption spectra, and shown that they provide a distinct optical fingerprint holding information pertaining to the blend layer thickness. By spectral fitting of the absorption spectra estimates for the blend layer thicknesses were obtained, the magnitude of which was generally smaller than the corresponding thicknesses determined by AFM. Optical simulations of solar cell absorption spectra for a wide range of blend layer thicknesses showed the expected linear relation between the position of a pronounced spectral minimum and the blend layer thickness. Likewise, relating the same minimum for the experimental absorption spectra to the blend layer thicknesses, but as determined by AFM, gave a linear but slightly different relation. The discrepancy between these relations most likely is due to the optical constants for the blend being derived with inappropriate model assumptions. This gives a small systematic error in thicknesses resulting from spectral fitting, in particular, for the solar cells where interference is outspoken. Nonetheless, we have demonstrated that the blend layer thickness of a P3HT:PCBM solar cell can be deduced from its absorption spectrum.

By optical simulations the absorption in the blend layer of the solar cell was derived and compared to the blend absorption spectra as derived from transmission spectra for the *s*- and *m*-type substrates. This showed that the latter substrates are appropriate neither for analyzing the light-harvesting properties of the blend in solar cells nor for the estimation of J_{sc}^{max}.

The solar cell performance with respect to η and J_{sc} increased with spin-coating speed as $1970 \rightarrow 630 \rightarrow 900 \rightarrow 1430$ rpm, in accord with J_{sc}^{max} obtained from optical simulations. The notable difference between J_{sc}^{max} and J_{sc} was uniquely linked to recombination in the solar cells. The simulated dependence of J_{sc}^{max} on blend layer thickness qualitatively agreed with most experimental findings in the literature despite differences in the P3HT:PCBM blend ratio employed.

Comparing blend layer thicknesses for *s*- and *m*-type and solar cell substrates, as inferred from spectral fitting and AFM measurements, did not lead to a firm conclusion as to the importance of differences in surface wetting properties of the substrates upon blend spin coating.

ACKNOWLEDGMENTS

Melanie Schumann is acknowledged for helping with the AFM measurements, the work group of Dr. Tiller for making available the Analytic Jena spectrometer, and B. Zimmermann and T. Fritz for valuable discussions. One of the authors (K.O.S) acknowledges Carlsbergfondet for financial support

[1] K. Inoue, R. Ulbricht, P. C. Madakasira, W. M. Sampson, S. Lee, J. Gutierrez, J. Ferraris, and A. A. Zakhidov, Synth. Met. **154**, 41 (2005).
[2] D. Chirvase, J. Parisi, J. C. Hummelen, and V. Dyakonov, Nanotechnology **15**, 1317 (2004).
[3] M. A. Ibrahim, O. Ambacher, S. Sensfuss, and G. Gobsch, Appl. Phys. Lett. **86**, 201120 (2005).
[4] V. Shrotriya, J. Ouyang, R. J. Tseng, G. Li, and Y. Yang, Chem. Phys. Lett. **411**, 138 (2005).
[5] V. D. Mihailetchi, H. X. Xie, B. de Boer, L. J. A. Koster, and P. W. M. Blom, Adv. Funct. Mater. **16**, 699 (2006).
[6] M. Reyes-Reyes, K. Kim, J. Dewald, R. Lopez-Sandoval, A. Avadhanula, S. Curran, and D. L. Carroll, Opt. Lett. **7**, 5749 (2005).
[7] P. Vanlaeke *et al.*, Sol. Energy Mater. Sol. Cells **90**, 2150 (2006).
[8] R. Cugola, U. Giovanella, P. Gianvincenzo, F. Bertini, M. Catellani, and S. Luzzati, Thin Solid Films **511–512**, 489 (2006).
[9] P. Vanlaeke, G. Vanhoyland, T. Aernouts, D. Cheyns, C. Deibel, J. V. Manca, P. Heremans, and J. Poortmans, Thin Solid Films **511–512**, 358 (2006).
[10] Y. Kim, S. A. Choulis, J. Nelson, D. D. C. Bradley, S. Cook, and J. R. Durrant, J. Mater. Sci. **40**, 1371 (2005).
[11] G. Li, V. Shrotriya, J. S. Huang, Y. Yao, T. Moriarty, K. Emery, and Y. Yang, Nat. Mater. **4**, 864 (2005).
[12] L. A. Pettersson, L. S. Roman, and O. Inganäs, J. Appl. Phys. **86**, 487 (1999).
[13] N.-K. Persson and O. Inganäs, in *Organic Photovoltaics: Mechanisms, Materials and Devices*, edited by S.-S. Sun and N. S. Sariciftci (CRC, Boca Raton, FL, 2005), Vol. 99, p. 107.
[14] H. Hoppe, N. Arnold, N. S. Sariciftci, and D. Meissner, Sol. Energy Mater. Sol. Cells **80**, 105 (2003).
[15] A. J. Moulé, J. B. Bonekamp, and K. Meerholz, J. Appl. Phys. **100**, 094503 (2006).
[16] H. Hoppe, S. Shokhovets, and G. Gobsch, Phys. stat. sol. (RLL) **1**, R40 (2007).
[17] L. H. Slooff, S. C. Veenstra, J. M. Kroon, D. J. D. Moet, J. Sweelssen, and M. M. Koetse, Appl. Phys. Lett. **90**, 143506 (2007).
[18] B. Zimmermann, M. Glatthaar, M. Niggemann, M. K. Riede, T. Ziegler, and A. Gombert, Proc. SPIE **6197**, 61970G (2006).
[19] D. W. Sievers, V. Shrotriya, and Y. Yang, J. Appl. Phys. **100**, 114509 (2006).
[20] F. Monestier *et al.*, Sol. Energy Mater. Sol. Cells **91**, 405 (2007).
[21] H. Hoppe, N. Arnold, D. Meissner, and N. S. Sariciftci, Thin Solid Films **451–452**, 589 (2004).
[22] N.-K. Persson, M. Schubert, and O. Inganäs, Sol. Energy Mater. Sol. Cells **83**, 169 (2004).
[23] N.-K. Persson and O. Inganäs, Sol. Energy Mater. Sol. Cells **90**, 3491 (2006).
[24] L. A. A. Pettersson, L. S. Roman, and O. Inganäs, J. Appl. Phys. **89**, 5564 (2001).
[25] G. Li, V. Shrotriya, Y. Yao, and Y. Yang, J. Appl. Phys. **98**, 043704 (2005).
[26] M. Riede, Ph.D. thesis, University of Konstanz, 2006.
[27] E. Palik, *Handbook of Optical Constants of Solids* (Academic, New York, 1985).
[28] M. G. Moharam and T. K. Gaylord, J. Opt. Soc. Am. **72**, 1385 (1982).
[29] M. G. Moharam and T. K. Gaylord, J. Opt. Soc. Am. A **71**, 811 (1981).
[30] P. Lalanne and G. M. Morris, J. Opt. Soc. Am. A **13**, 779 (1996).
[31] P. Lalanne and M. P. Jurek, J. Mod. Opt. **45**, 1357 (1998).
[32] M. Niggemann, M. Glatthaar, A. Gombert, A. Hinsch, and V. Wittwer, Thin Solid Films **451**, 619 (2004).
[33] P. Schilinsky, C. Waldauf, and C. J. Brabec, Appl. Phys. Lett. **81**, 3885 (2002).
[34] H. Hoppe, N. Arnold, D. Meissner, and N. S. Sariciftci, Synth. Met. **143**, 113 (2004).
[35] M. Reyes-Reyes, K. Kim, and D. L. Carroll, Appl. Phys. Lett. **87**, 083506 (2005).
[36] W. L. Ma, C. Y. Yang, X. Gong, K. Lee, and A. J. Heeger, Adv. Funct. Mater. **15**, 1617 (2005).